# School of Biomedical Engineering, Science, and Health Systems

# Evaluation and Application of a RBF Neural Network for Online Single-Sweep Extraction of SEPs During Scoliosis Surgery

Anna C. Merzagora*, *Student Member, IEEE*, Francesco Bracchi, Sergio Cerutti, *Fellow, IEEE*, Lorenzo Rossi, Alberto Gaggiani, and Anna M. Bianchi, *Member, IEEE*

***Abstract*—A method for on-line single sweep detection of somatosensory evoked potentials (SEPs) during intraoperative neuromonitoring is proposed. It is based on a radial-basis function neural network with Gaussian activations. In order to improve its tracking capabilities, the radial-basis functions location is partially learnt sweep-by-sweep; the training algorithm is effective, though consistent with real-time applications. This new detection method has been tested on simulated data so as to set the network parameters. Moreover, it has been applied to real recordings obtained from a new neuromonitoring technique which is based on the simultaneous observation of the SEP and of the evoked H-reflex elicited by the same electric stimulus. The SEPs have been extracted using the neural network and the results have then been compared to those obtained by ARX filtering and correlated with the spinal cord integrity information obtained by the H-reflex. The proposed algorithm has been proved to be particularly effective and suitable for single-sweep detection. It is able to track both sudden and smooth signal changes of both amplitude and latency and the needed computational time is moderate.**

***Index Terms*—EP, H-reflex, neural network, neuromonitoring, RBFNN, SEP, single sweep, single trial.**

## I. Introduction

THE use of somatosensory evoked potentials (SEPs) for the intraoperative monitoring of the functionality of the spinal cord is well known and its usefulness is confirmed by the literature [1]–[3]. Recordings that diverge from normality can be interpreted as manifestation of suffering of the spinal cord. A prompt detection of these variations enables the surgeon to modify or suspend the operative procedure accordingly, in order to avoid temporary or permanent neurological deficits due to accidental damage of the nervous tissue. For this reason, the single-sweep extraction of SEPs has been suggested as particularly useful [4], [5]. In this paper, a method for the single-sweep detection of SEPs is presented. "Wiener" filtering was among the first algorithms to be used for single-trial SEP extraction, because of its optimality in terms of mean square error. The "Wiener" filtering, however, requires *a priori* knowledge about the spectra of signal and noise and the signals are also supposed to be stationary. Other traditional algorithms are based on adaptive models. Their main drawback is that they assume a linear signal generation model. The method presented is, instead, based on the algorithm described in [4], [6] for visual evoked potentials (VEPs) and brain-stem auditory evoked potentials (BAEPs): it consists of a radial-basis function neural network (RBFNN) with Gaussian activation functions. The new method offers enhanced capability in tracking latency changes: the innovation here proposed is the adaptivity of the Gaussian functions centers, realized through a simple but quick and effective method. In this way, the latency and amplitude of the underlying SEP are better identified and their evaluation is more reliable. This method is applied in a recently proposed neuromonitoring technique that is based on the simultaneous observation of the SEP (in particular its main peak occurring after about 30 ms, called P30) and of the evoked H-reflex elicited by the same electrical stimulus [5]. Like others combined neuromonitoring modalities [7]–[9], this technique capitalizes on the fact that these two signals monitor different nervous pathways [10] whose functionality can be altered by the same surgical maneuvers [11]. SEPs in fact investigate the sensory pathways, while the H-reflex investigates part of the sensory pathways, part of the motor pathways (i.e., downward from where the reflex circuit is located) and indirectly the facilitatory descending pathways.

Manuscript received October 18, 2005; revised October 22, 2006. This work was supported by the Contratto Convenzione Ricerca under Grant CAP 7-9-39. *Asterisk indicates corresponding author.*

*A. C. Merzagora was with the Biomedical Engineering Department, the Polytechnic University of Milan, 20136 Milan, Italy. She is now is with the School of Biomedical Engineering, Science and Health Systems, Drexel University, 3141 Chestnut Street, Philadelphia, PA 19104 USA (e-mail: a.merzagora@drexel.edu).

F. Bracchi is with the Institute of Human Physiology II, University of Milan Medical School, 20157 Milan, Italy (e-mail: francesco.bracchi@unimi.it).

A. Gaggiani is with the University of Milan Medical School, 20157 Milan, Italy.

S. Cerutti, A. M. Bianchi, and L. Rossi are with the Department of Biomedical Engineering, Polytechnic University of Milan, 20136 Milan, Italy (e-mail: cerutti@biomed.polimi.it; annamaria.bianchi@polimi.it; lorenzo.rossi@biomed.polimi.it)

Digital Object Identifier 10.1109/TBME.2006.889770

## II. Method

### A. RBFNNs: General Principles

Radial-basis function neural networks represent a particular category of unbiased feedforward neural networks with the following three layers:

— an input layer, consisting of an instant input vector $\mathbf{X}^{(\mathrm{p})}$ with $p$ elements;

— a hidden layer with $N$ neurons;

— an output layer, usually comprised of only one neuron.

A scheme of the network is shown in Fig. 1.

The input weights are generally set to 1, whereas weights between the hidden layer and the output node are adaptively learnt as the signal processing goes on.

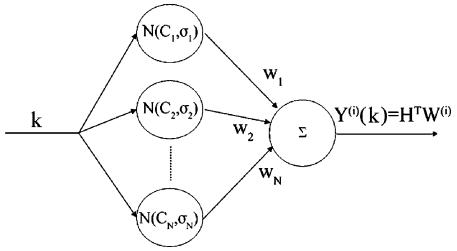


Fig. 1. The RBFNN used for single-sweep detection of SEPs is a feed-forward network with three layers and Gaussian activation functions for the hidden nodes. $N(\mathrm{C}_j, \sigma_j)$ indicates a Gaussian function with center in $\mathrm{C}_j$ and spread $\sigma_j$.

The activation function of the hidden layer is the same for all its nodes and it is a function $F$ with radial symmetry. The radial-basis function $F_j$ of the $j$th node is characterized by a center vector $\mathbf{C}_j$ (with $p$ elements) and by a radius $d_j$ that represents the Euclidean distance between the generic instant input vector $\mathbf{X}^{(p)}$ and the center vector $\mathbf{C}_j$. The radial-basis function is maximum (usually equal to 1) when the radius is 0, i.e., when the input and the center of the node coincide, and should decrease as the radius increases. The output of the $j$th hidden neuron is the value of the radial function evaluated for the radius $d_j$: $h_j(\mathbf{X}^{(p)}) = F(\mathbf{X}^{(\mathrm{p})}, \mathbf{C}_j) = F(d_j)$.

The responses of the $N$ hidden neurons feed the output unit, which combines them in a weighted sum to form the global network output in accordance with

$$Y(\mathbf{X}^{(p)}) = \sum_{j=1}^{N} w_j \cdot h_j(\mathbf{X}^{(p)}) \tag{1}$$

where $w_j$ represents the weight between the $j$th hidden node and the output neuron.

The weights are learnt in a supervised way, which consists in comparing the network output and a reference signal and minimizing the difference between these two.

The most commonly used radial-basis function is the Gaussian function [12], [13]

$$F(\mathbf{X}, \mathbf{C}_j) = \mathrm{e}^{-(|\mathbf{X}-\mathbf{C}_j|/\sigma_j)^2} \tag{2}$$

where $\sigma_j^2$ is the spread and $\mathbf{C}_j$ acts as a mean. Clearly, the use of a Gaussian activation function makes the mapping from the input layer to the hidden layer nonlinear. It is due to these Gaussian functions that the RBFNN goes beyond the limits of traditional adaptive filters and linear models [4], [6].

### *B. Specific Architecture for SEP Detection*

For the specific application of RBFNNs to single-sweep detection of SEPs, a particular configuration of the network is required. Fig. 1 shows the overall architecture of the considered neural network. First of all, the instant input is not a vector but a scalar: it is the discrete time, i.e., the number of the current sample in the sweep, after the stimulus. So, if the acquired sweep is formed by $M$ samples, the total input vector for each sweep is $[1 \ldots k \ldots M]$, where 1 represents the stimulus delivery instant and $M$ is the end of the single recording; the instant scalar input, instead, is $k$. The centers of the $N$ Gaussian functions are no more located in a $p$-dimensional space but are distributed over the discrete time axis that goes from 1 to $M$. Therefore, the network output is computed as follows:

$$\mathbf{Y}^{(i)}(k) = \sum_{j=1}^{N} w_j^{(i)} \cdot h_j(k) = \sum_{j=1}^{N} w_j^{(i)} \mathrm{e}^{-\left(\left|k-\mathrm{C}_j^{(i)}\right|/\sigma_j\right)^2} = \mathbf{H}^{\mathrm{T}}\mathbf{W}^{(i)}. \tag{3}$$

After the learning of the proper network parameters (as shown in the next Section II-C), the output $Y^{(i)}(k)$ represents the $k$th sample of the detected SEP for the $i$th sweep; $w_j^{(i)}$ is the current weight between the $j$th node and the output unit. $\mathrm{C}_j^{(\mathrm{i})}$ is, instead, the scalar center of the $j$th neuron for that sweep.

Obviously, the performance in the single-sweep detection of SEPs is tightly connected with the parameters that describe the network in detail. In common applications such parameters are fully learnt, but that would require a high computational time, inconsistent with real-time applications. For this reason, some simplifications have been proposed, though maintaining the global learning capability of the network. In particular, the following.

*1) Number of Neurons:* The number of hidden units depends on the waveform of the signal to be detected and has to be experimentally found.

*2) Centers of the Gaussian Functions:* At the beginning, the centers of the Gaussian functions are uniformly distributed over the discrete time axis, as described by

$$\mathrm{C}_j = (j-1)\left(\frac{M-1}{N-1}\right) + 1 \quad j = 1 \text{ to } N. \tag{4}$$

However, the detection of the latency of the P30 peak is particularly important for intraoperative neuromonitoring and the better a Gaussian function is centered on the P30 peak, the more accurate is its latency identification. This can be achieved in two ways: using a high number of unmoved Gaussian functions, i.e., of neurons (as suggested in [6]) or, with a lower number of neurons, moving adaptively the Gaussian functions themselves. The first solution requires a high computational time; for this reason, it has been preferred to initialize the centers as described in (4) and then adjust their locations adaptively sweep-by-sweep. In order to keep the computational time moderate for real-time applications, the centers are not adapted independently one from another, but the whole array is shifted till the best identification of the SEP latency is achieved, as will be described in more detail in Section II-C.

*3) Spreads of the Gaussian Functions:* In order to reduce the computational time, the spreads are not learnt, but previously fixed and kept unchanged. For further model simplification, the spread is the same for all the hidden activation functions, as it has been demonstrated that RBFNNs with such a characteristic do not loose their universal approximation capability [12], [13]. Clearly, this spread is connected with the number of hidden units

and with the number of samples to be spanned. Moreover, this unique spread should obviously balance the abilities to follow both the low-frequency and the high-frequency components of the signal to be detected; this compromise is achieved through the experimental parameter $\beta$

$$\sigma = \beta \left( \frac{M-1}{N-1} \right). \tag{5}$$

### C. Network Learning

The single-sweep detection of SEPs using this RBFNN is performed by letting the network learn continuously the weights $w_j$ and the centers' location of the Gaussian functions that characterize the hidden layer. In order to perform such adjustments, some theoretical hypotheses regarding the signal to be processed are required. Indeed, if considering the recording $\mathrm{R(t)}$, in which the underlying evoked signal $S(\mathrm{t})$ is embedded in the electroencephalographic noise $N(\mathrm{t})$, the hypotheses are mainly three: additivity of signal and noise; noncorrelation of signal and noise; null mean of the noise. Obviously, the hypotheses listed above cannot be regarded as completely correct, in particular the noncorrelation of signal and noise, but they are commonly accepted for other detection algorithms and for EP analysis [4], [14]–[18].

On the basis of these hypotheses, the sweep-by-sweep adaptation is performed through a supervised algorithm: the minimization of the mean square error (mse) between the current recording and the network output. At each trial the total network output vector $\mathbf{Y}^{(i)}$ and the real recording vector $\mathbf{R}^{(i)}$ (consisting of the signal $\mathbf{S}^{(i)}$ and the noise $\mathbf{N}^{(i)}$ ) are compared and the mse is computed as follows:

$$\begin{aligned} &\mathrm{E}\left[\left(\mathbf{R}^{(i)}-\mathbf{Y}^{(i)}\right)^{\mathrm{T}}\left(\mathbf{R}^{(i)}-\mathbf{Y}^{(i)}\right)\right] \\ &=\mathrm{E}\left[\left(\mathbf{S}^{(i)}-\mathbf{Y}^{(i)}\right)^{\mathrm{T}}\left(\mathbf{S}^{(i)}-\mathbf{Y}^{(i)}\right)\right]+\mathrm{E}\left[\mathbf{N}^{(i)\mathrm{T}}\cdot\mathbf{N}^{(i)}\right] \end{aligned} \tag{6}$$

if $\mathbf{N^{(i)}}$ and $\mathbf{S^{(i)}}$ are thought uncorrelated, as previously stated. Therefore, as $\mathrm{E}[\mathbf{N}^{(i)\mathrm{T}}\,\mathbf{N^{(i)}}]$ can be regarded as independent of the weight vector $\mathbf{W}^{(i)}$ and of the centers location, the mse is minimized when $\mathrm{E}[\mathbf{Y}^{(i)}]$ tends to $\mathbf{S}^{(i)}$.

More in detail, the adaptation follows two steps: the first is connected with the learning of the centers location, the second is connected instead with the learning of the weights. With regard to the centers' location, it is learnt iteratively; the aim is to shift gradually the whole array of Gaussian functions in order to span the interval between two centers as set in accordance with (4). Maintaining the space relations between the centers prevents the functions from being too distant one from another; moreover, major differences between the real SEP and the estimated one are concentrated at the beginning or at the end of the detected signal (as Gaussian functions may leave a poorly covered signal portion at the extremities), thus not affecting the identification of the P30 peak. The iteration step is set to 1 sample (the time resolution obviously depends on the acquisition settings).

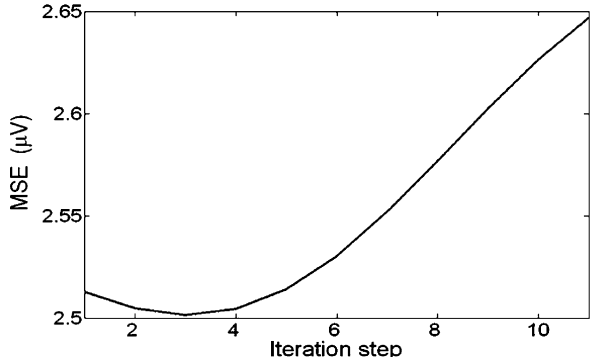


Fig. 2. The trend of the mse obtained when shifting the centers array is smooth and without local minima.

At the beginning the centers are distributed in accordance with (4). The centers array is then shifted of one sample and the mse is evaluated. In order to realize the adaptation, the algorithm steps are the following:

— the mse is computed;

— if the current mse is smaller than that of the previous step, the centers location is shifted of one more sample and the algorithm restarts at the previous step; otherwise, if the current mse is larger than that at the first step, the centers location is shifted back of one sample and the algorithm stops.

Obviously, the centers are, at most, shifted of as many steps as the number of samples between two consecutive centers: the algorithm does not proceed if the center $\mathrm{C}_j$ is now where center $\mathrm{C}_{j+1}$ was at the beginning of the adaptation algorithm. Even if it is possible, from the theoretical point of view, that the results of this heuristics are not global minima, it has been found that the error trend, when shifting over the interval between two consecutive centers, is generally smooth and without local minima, as shown in Fig. 2.

As far as the adaptation of the weights is concerned, the convergence to the optimal weights is achieved through the least mean squares algorithm [19]

$$\mathbf{W}^{(i+1)} = \mathbf{W}^{(i)} + 2\eta\mathbf{R}\left(\mathbf{D}^{(i)} - \mathbf{Y}^{(i)}\right) \tag{7}$$

where the index $i$ denotes the $i$th sweep. The parameter $\eta$ represents the convergence rate: it controls the speed of adaptation and the convergence stability.

Thus, applying the described adaptation method, both the weights and the centers location are learnt and the network output is optimized.

### D. Setting of the Network Parameters

The performance of the whole algorithm strongly depends on the value of its parameters, i.e., the number of hidden neurons $N$, the spread factor $\beta$ and the convergence rate $\eta$. The best values for them have been set on the basis of simulations whose concept is described in Section III-C. For the choice of each parameter, the following two figures of merit were taken into consideration:

TABLE I
CHOICE OF THE NUMBER OF HIDDEN NEURONS

| Number of neurons | Normalized mse | Correlation coefficient |
|---|---|---|
| 10 | 0.1245 | 0.8277 |
| 20 | 0.0911 | 0.8747 |
| 25 | 0.0834 | 0.8910 |
| 30 | 0.0793 | 0.8993 |
| 35 | 0.0784 | 0.9034 |
| 40 | 0.0766 | 0.9102 |
| 50 | 0.0741 | 0.9188 |
| 60 | 0.0724 | 0.9256 |

The values of the normalized mse and of the correlation coefficient suggest the use of a high number of hidden nodes. but that would increase greatly the computational time.

TABLE II
CHOICE OF THE SPREAD FACTOR

| β | Normalized mse | Correlation coefficient |
|---|---|---|
| 0.1 | 0.1447 | 0.4851 |
| 0.3 | 0.1013 | 0.8057 |
| 0.5 | 0.0793 | 0.8993 |
| 0.7 | 0.0977 | 0.8738 |
| 0.7 | 0.1300 | 0.8363 |

The here summarized simulation results show that 0.5 is the best value for β, as it minimizes the mse and maximizes the correlation coefficient.

— the normalized mse (nmse), computed as

$$\text{nmse} = \frac{\sqrt{\frac{1}{M}\sum_{k=1}^{M}(S(k)-Y(k))^2}}{[\max(S)-\min(S)]} \tag{8}$$

where $S$ is the simulated underlying signal in the recording (i.e., the reference SEP) and $Y$ is the network output;

— the correlation coefficient $\rho$ between the network output and the reference SEP.

Now the single factors will be analyzed.

*1) Number of Neurons:* As expected, the simulation results presented in Table I show that a high number of neurons allows a better detection of the underlying signal, both in terms of nmse and correlation coefficient. Nevertheless, the use of many hidden neurons would obviously increase greatly the computational time. As the algorithm is meant for real-time applications, the computational time needed by the algorithm to produce the estimated evoked potential is a most important factor. A good compromise between accuracy and velocity is obtained with 30 neurons. Furthermore, it could be seen in Table I that with 30 neurons the nmse has already decreased considerably and the correlation coefficient has already reached an almost stable value.

*2) Spread Factor:* The same evaluation methods as before have been applied to the spread factor $\beta$. On the basis of the simulation results presented in Table II, 0.5 is the best value, both in terms of nmse and correlation coefficient.

*3) Convergence Rate:* The simulation, whose results are shown in Table III, suggests the use of a low convergence rate, because in this way the system is less affected by abrupt changes and noise. Conversely, a high convergence rate enables the system to better track the trial-to-trial variabilities. For this reason, even if the results seem to be better with lower values of $\eta$, with such values the adaptivity of the network would be seriously diminished and it would require a considerably longer time to converge. For this reason, $\eta = 0.0035$ was chosen.

TABLE III
CHOICE OF THE CONVERGENCE RATE

| η | Normalized mse | Correlation coefficient |
|---|---|---|
| 0.0010 | 0.0673 | 0.9421 |
| 0.0020 | 0.0701 | 0.9260 |
| 0.0030 | 0.0759 | 0.9079 |
| 0.0035 | 0.0793 | 0.8993 |
| 0.0040 | 0.0827 | 0.8914 |
| 0.0050 | 0.0894 | 0.8778 |
| 0.0060 | 0.0964 | 0.8661 |

Even if a low convergence rate seems to offer better results, it would compromise the learning ability of the network.

After the network parameters have been set, the weights have been trained over a set of simulated sweeps in order to obtain reasonable values for the initialization of the network. In this way, the initial learning of the weights during real surgery is faster and a lower number of sweeps is needed for initialization.

## III. MATERIALS

### A. Clinical Protocol

The analyzed data consist of electroencephalogram (EEG) recordings (containing the evoked responses) and electromyogram recordings (containing the H-reflex responses) acquired during 13 idiopathic scoliosis surgeries. The experimental settings, used to elicit both the H-reflex and the SEPs during surgery and to acquire the two signals, are as follows:

*1) Stimulation:* The stimulated nerve is the posterior tibial nerve at the popliteal fossa, where the nerve fibers run more superficially: the cathode is at the popliteal fossa and the anode over the patella. The electrical stimulus is a constant voltage rectangular impulse with a duration set to 1 ms. The repetition frequency of the pulses is 0.1 Hz (the long interstimulus interval is necessary to extinguish the transient spinal excitatory/inhibitory phenomena which last from 5 to 7 s after each stimulus) [20]. The current intensity range for stimulation is between 3 and 50 mA; it is set for each patient to obtain a medium amplitude H-reflex wave. If necessary, it is varied during the surgery.

*2) Acquisition:* The acquisition of SEPs is performed through needle electrodes set on the scalp in Cz', with a reference at the ear lobe. The reference electrode for the H-reflex recording is over the Achilles tendon and the filter used for the SEPs before the analog-to-digital conversion is set as follows: low cutoff frequency 1 Hz; high cutoff frequency 300 Hz. With regard to the H-reflex, the settings are: low cutoff frequency 30 Hz; high cutoff frequency 10 kHz. The sampling frequencies for the SEPs and the H-reflex are 2560 Hz and 10 240 Hz, respectively. The duration of the sampled time interval is 125 ms for the SEP and 62.5 ms for the H-reflex.

TABLE IV
CLINICAL CASES DATA

| Case | Age | Sex | Level | Number of accepted sweeps | Acceptation rate % |
|---|---|---|---|---|---|
| 1 | 13 | M | D3-L3 | 238 | 31.6 |
| 2 | 20 | F | D5-L3 | 455 | 54.8 |
| 3 | 14 | F | D4-L4 | 461 | 44.5 |
| 4 | 22 | M | D3-L3 | 703 | 58.8 |
| 5 | 53 | F | D4-L4 | 348 | 36.4 |
| 6 | 59 | F | D5-L5 | 505 | 38.3 |
| 7 | 51 | F | D4-L5 | 607 | 56.3 |
| 8 | 17 | F | D2-L3 | 609 | 59.5 |
| 9 | 26 | F | D3-L4 | 298 | 39.8 |
| 10 | 45 | F | D4-L4 | 301 | 29.4 |
| 11 | 57 | F | D4-L4 | 424 | 47.5 |
| 12 | 22 | M | D3-D12 | 515 | 54.4 |
| 13 | 23 | F | D3-L3 | 257 | 31.2 |

Characterization of the 13 clinical cases, with age and sex of the patient and with indication of the vertebral level of the scoliosis.

In Table IV, data characterizing the 13 clinical cases are summarized. The subjects' mean age is 32.5 years and the standard deviation is 17.5 years.

### B. Analysis Protocol

Before data processing, the sweeps found to be corrupted (e.g., because of the interference of the electrotome) have been rejected. Then, an initial adaptation of the RBFNN weights is necessary. At the beginning the weights are initialized with standard values obtained as previously described (see Section II-D). Their purpose is to improve the algorithm performance, by reducing the time needed to converge to the subject-specific weights. The first 50 sweeps are used for the preliminary adaptation of the weights and to obtain a reference SEP. That reference is used to evaluate the initial amplitude and latency in order to asses the percentage variations throughout the surgery. The SEPs are then detected and their amplitudes and latencies analyzed along with those of the H-reflex and with the trend of the patient's body temperature. The performed statistical analyses regard the mean and standard deviation of SEPs and H-reflex, and the Pearson's Product Moment Correlation Coefficient ($r$) between the trends of amplitudes and latencies of the two monitored signals.

### C. Simulation Protocol

The performance of the proposed method for the single-sweep detection of SEPs has been studied and assessed by processing real data and through *ad hoc* simulations. To this purpose real recordings have been used to create fictitious registrations. This is necessary because, in order to evaluate the exactness of the signal estimated by the algorithm, the underlying signal must be known. To avoid the stimulation artifact, the first 4 ms of the recording after stimulus application were not considered, thus obtaining vectors of 310 samples.

A reference SEP was then obtained by averaging a hundred real records. The EEG had to be simulated: for this purpose an autoregressive (AR) model was used [21], [22] and the optimal order was evaluated with the AIC method. The parameters were estimated analyzing real EEG recordings; then the output of this white-noise-driven AR process was band-passed with an equiripple filter whose parameters complied with the real acquisition filter. Adding the simulated EEG and the reference SEP, complete registrations have been reproduced. The analysis of the mse and of the correlation between the network output and the reference SEP was performed.

The fine tuning of the network parameters based on the simulated recordings has already been presented in Section II-D.

## IV. RESULTS

The method described in Section II has been applied to 13 cases and the results are summarized in Tables V and VI. In particular, Table V provides the mean amplitude, the amplitude standard deviation and the mean latency of both SEPs and HR for each of the 13 cases. It also provides the Pearson's Correlation Coefficients ($r$) between the amplitude of the HR and those of the SEPs extracted with the RBFNN; the coefficient $r$ is computed as follows:

$$r = \frac{\sum_{i=1}^{F} (\mathrm{A}_{\mathrm{X}}^{(i)} - \overline{\mathrm{A}}_{\mathrm{X}})(\mathrm{A}_{\mathrm{Z}}^{(i)} - \overline{\mathrm{A}}_{\mathrm{Z}})}{\sqrt{\sum_{i=1}^{F} (\mathrm{A}_{\mathrm{X}}^{(i)} - \overline{\mathrm{A}}_{\mathrm{X}})^2 \cdot \sum_{i=1}^{F} (\mathrm{A}_{\mathrm{Z}}^{(i)} - \overline{\mathrm{A}}_{\mathrm{Z}})^2}} \tag{10}$$

where $\mathrm{A}_{\mathrm{X}}^{(i)}$ and $\mathrm{A}_{\mathrm{Z}}^{(i)}$ denote two variables of interest at the $i$th sweep; $\overline{\mathrm{A}}_{\mathrm{X}}$ and $\overline{\mathrm{A}}_{\mathrm{Z}}$ are the means of the variable of interest across sweeps; $F$ the total number of sweeps.

Particular attention has also been paid to the effects of surgical maneuvers on SEPs and HR. Fig. 3(a) and (b) shows the monitored signal after the insertion of sublaminar hooks in two different positions, i.e., under or close to where the H-reflex circuit is located.

In order to better understand the information that can be obtained from the combined monitoring system and from the application of this new single-sweep extraction method, detailed results obtained for one case (case 1) are presented.

In particular, the results found from this case using the RBFNN have been compared with those found with the ARX filtering [14], as it is particularly suitable for single-sweep detection of SEPs. The ARX model was driven by a moving average of the recorded sweeps weighted by an exponential window with a forgetting factor 0.95 [5]; the optimal orders found with the AIC method were $[\mathrm{n}, \mathrm{m}, d] = [4, 2, 1]$. The total number of available sweeps after the first rejection was 238, but a further analysis due to the poor results of the ARX filtering was necessary, so the actual number of sweeps was reduced to 185. The reference SEPs obtained by the two algorithms using the sweeps available before the first surgical maneuvers (Fig. 4) have slightly different amplitudes and latencies one from another: 5.99 $\mu$V and 31.73 ms, respectively using the RBFNN and 5.34 $\mu$V and 32.03 ms using the ARX filter. Fig. 5(a) shows the urine bladder temperature throughout the surgery and a constant decrease can be seen. In Fig. 5(c), both the detection algorithms indicate a latency increase. Finally, Fig. 5(c) shows the amplitudes detected by the two algorithms and they are related to the HR amplitudes.

Statistical values about the amplitudes and latencies obtained by the RBFNN and the ARX filter in case 1 are summarized in

TABLE V
STATISTICAL VALUES OF THE PROCESSED CLINICAL CASES

| Case | SEP amplitude (μV) | Mean SEP latency (ms) | HR amplitude (mV) | Mean HR latency (ms) | Pearson's Correlation Coefficient (r) | Degrees of Freedom |
|---|---|---|---|---|---|---|
| 1 | 5.301 ± 1.128 | 34.31 | 9.479 ± 2.493 | 35.83 | 0.396 | 236 |
| 2 | 8.723 ± 2.896 | 34.45 | 5.648 ± 1.662 | 40.20 | 0.348 | 453 |
| 3 | 6.020 ± 1.295 | 29.62 | 6.254 ± 1.985 | 34.77 | 0.367 | 459 |
| 4 | 2.615 ± 0.744 | 33.83 | 5.925 ± 1.202 | 35.57 | 0.263 | 701 |
| 5 | 4.423 ± 1.041 | 35.41 | 5.669 ± 1.262 | 39.19 | 0.562 | 346 |
| 6 | 5.240 ± 1.460 | 35.14 | 4.073 ± 2.045 | 35.13 | 0.293 | 503 |
| 7 | 4.122 ± 0.731 | 34.11 | 3.389 ± 0.757 | 35.89 | 0.186 | 605 |
| 8 | 5.742 ± 1.569 | 34.64 | 0.540 ± 0.368 | 37.31 | 0.503 | 607 |
| 9 | 3.168 ± 1.019 | 30.16 | 6.824 ± 0.946 | 30.97 | 0.399 | 296 |
| 10 | 4.426 ± 1.412 | 36.89 | 1.519 ± 0.879 | 39.25 | 0.382 | 299 |
| 11 | 4.570 ± 1.342 | 34.62 | 4.019 ± 0.817 | 35.10 | 0.302 | 422 |
| 12 | 4.717 ± 1.413 | 42.06 | 6.826 ± 1.578 | 40.02 | 0.219 | 513 |
| 13 | 4.408 ± 1.506 | 36.73 | 5.997 ± 1.087 | 39.51 | 0.294 | 255 |

Values of the features extracted from the monitored signals: amplitude and latency of the P30 peak for SEP; amplitude and latency of the H wave for the H-reflex. Also, for each case the degrees of freedom and the Pearson's correlation coefficients between SEP and HR amplitude trends are listed.

TABLE VI
COMPARISON BETWEEN RBFNN AND ARX.

| Parameter | |
|---|---|
| Mean SEP amplitude (RBFNN) | 5.301 μV |
| Standard deviation SEP amplitude (RBFNN) | 1.128 μV |
| Mean SEP amplitude (ARX) | 4.521 μV |
| Standard deviation SEP amplitude (ARX) | 1.752 μV |
| Degrees of freedom | 183 |
| r SEP amplitude trends RBFNN-ARX | 0.3788 (**) |
| r SEP latency trends RBFNN-ARX | 0.8884 (**) |
| r HR – SEP amplitude trend (RBFNN) | 0.3959 (**) |
| r HR – SEP amplitude trend (ARX) | 0.1825 (*) |
| r HR – SEP latency trend (RBFNN) | 0.1264 |
| r HR – SEP latency trend (ARX) | 0.1064 |

Values about SEPs extracted with both the RBFNN and the ARX filtering and about HR in case 1. (**) and (*) indicate statistical significance respectively at 99% and 95%.

Table IV. Particular stress is laid on the Pearson's Correlation Coefficients ($r$) between the values found by the two algorithms.

For the considered degrees of freedom, the minimum $r$ values in order to have a significant correlation at 95% and 99% of confidence are 0.143 and 0.188, respectively [23].

## V. DISCUSSION

The new method proposed for the single-sweep extraction of SEPs has been evaluated through its application to 13 clinical cases and the results are presented in Section IV. The first parameter that has been investigated is the Pearson's Correlation Coefficient between the amplitude trends of SEPs and HR. Indeed, a good analysis can be performed comparing the extracted SEPs with the trend of the HR when real underlying SEPs are unknown. This is due to the fact that HR and SEPs monitor different pathways that are involved in the same surgical maneuvers [10], [11]. As shown in Table V, the Pearson's Correlation Coefficient offered by the RBFNN is significant in all the 13 considered cases in relation to the degrees of freedom [23]. The next crucial aspect to be considered was the responsiveness of the RBFNN to the sudden changes caused by surgical maneuvers performed on the column, such as hammer-strokes or traction and the results strengthen the already stated need of a combined neuromonitoring. In particular, it has been found that

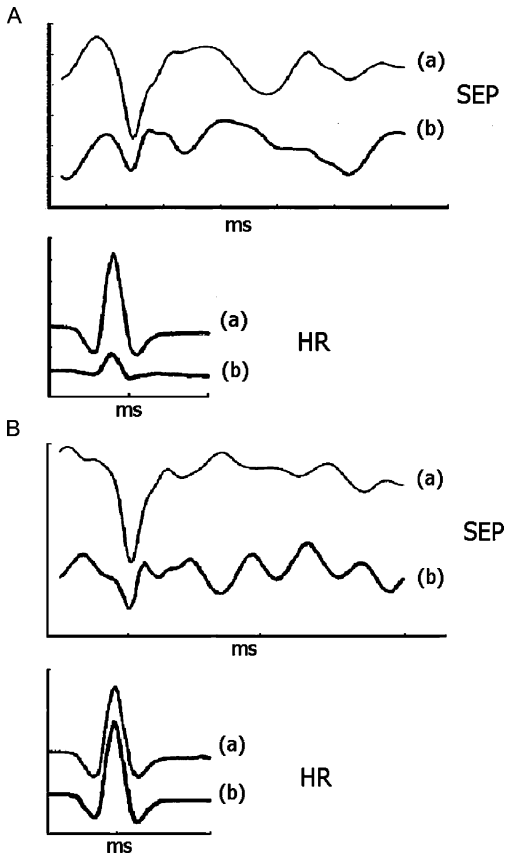


Fig. 3. In (A) (top), the black lines (b) show the effects of the insertion of a sublaminar hook at D8, while gray lines (a) display the waveforms before the insertion. Both SEP and HR are affected. In (B) (bottom), the black lines (b) show the effects of the insertion of a sublaminar hook at D1, while gray lines (a) display the waveforms before the insertion. Only the SEP is affected, as the maneuvers do not involve the H-reflex neural pathways.

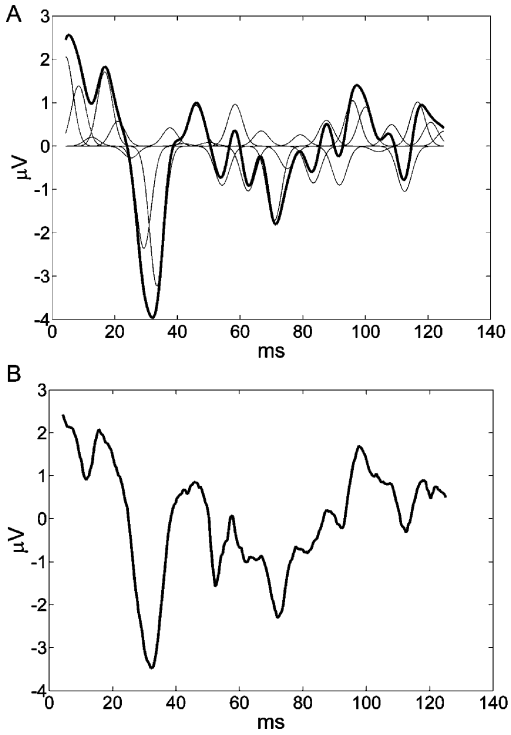


Fig. 4. Reference SEPs extracted with RBFNN (top) and ARX filter (bottom). In the RBFNN reference, the Gaussian functions that are summed to build the output are also displayed.

the insertion of sublaminar hooks close to the reflex circuit location affects both the SEPs and the H-reflex [see Fig. 3(a)]; on the contrary, when the hooks are inserted above the reflex circuit location, only the SEPs show an amplitude fall, as shown in Fig. 3(b): in this case, in fact, the nervous fibers involved in the H-reflex generation are no more functionally affected by the maneuver, so no decrement occurs. The aim of neuromonitoring, in fact, is to detect a possible alteration of the spinal cord functionality through observation of excitability changes of the nervous fibers involved in the generation of the monitored signals.

For a better insight of the usefulness of the proposed extraction algorithm, detailed results for one case have also been offered. The total number of sweeps analyzed in the considered case is 185, which represents a statistically significant number, therefore strengthening the conclusions suggested on the basis of the obtained results. When comparing the performances of the RBFNN and the ARX model, the correlation between the amplitude of the H-reflex and that of the SEP is significant for both methods, even if that obtained by the RBFNN is higher ($p = 0.01$ for RBFNN and $p = 0.05$ for ARX) (see Table VI). Moreover, the correlation between the amplitudes and latencies found by both ARX and RBFNN are strong though slightly different (see Table VI). Thus, even if the network offers a better correlation with the H-reflex trends, the results of the ARX filter are somewhat similar to those of the network.

Fig. 5(a) shows the urine bladder temperature trend, which is a most important factor to be considered in correlation with the latency trends shown in Fig. 5(b). The urine bladder temperature gives information about the patient's body temperature and, when a wide portion of the vertebral column is exposed, it

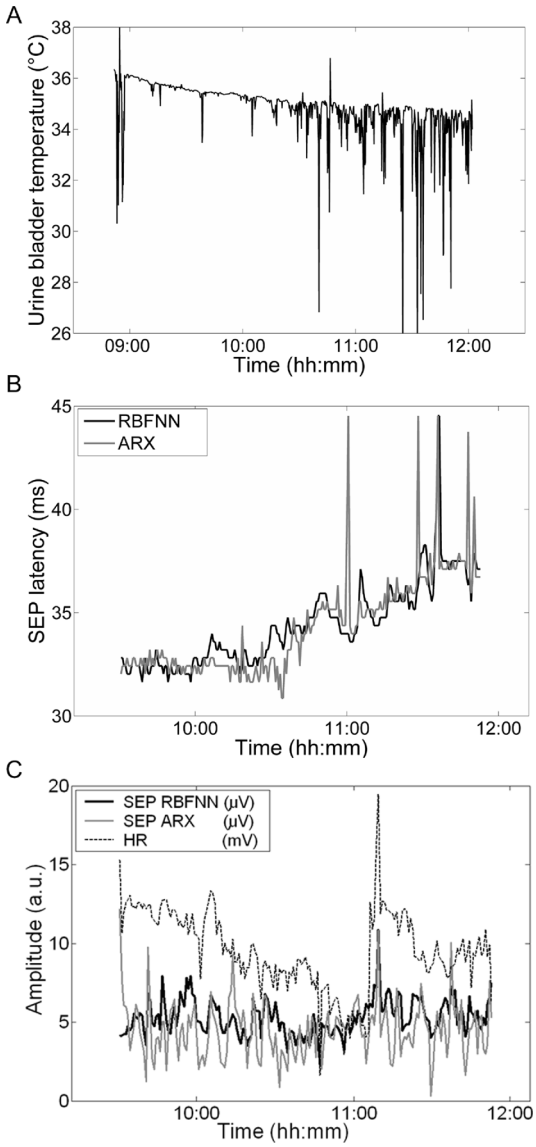


Fig. 5. The graph at the top (a) shows the urine bladder temperature; the peaks are due to interference caused by the electrosurgical equipment. The other two graphs show the (b) SEP latencies and (c) amplitudes obtained by the two detection algorithms. In (c), the H-reflex amplitude is reported. Crucial maneuvers: 10:00 – sequence of hammer-strokes; 10:30 – column traction.

may have slightly different dynamics from the epidural temperature for which, instead, an inverse relation to the SEP latency has been proved [24]. Nonetheless, an overall latency increase corresponds to an overall temperature decrease in Fig. 5. It is also evident that the false latency identifications present in the case of the ARX filtering are not shown using the RBFNN; problems in the identification remain only at the end of the surgery. In Fig. 5(c), the amplitudes of the H-reflex and those of the SEPs detected by the two algorithms are plotted together. As it can be seen from the evolutions of amplitudes and latencies throughout the surgery, a strong relation between amplitude and latency is present. It can be seen in Fig. 5(b) and (c) just after 10:00, as a consequence of hammer-strokes, and between 10:30 and 11:00, as a consequence of column traction: there is a latency increase along with an amplitude fall.

## VI. Conclusion

The aim of this study was to investigate the applicability of RBFNNs for on-line single sweep extraction of SEPs. The algorithm has been tuned on simulated data; moreover, results are provided about the algorithm application to real data.

With reference to the simulations and comparisons described above, the conclusions that can be drawn are mainly three.

The first is that, after the comparison between the RBFNN performance and that of the ARX filtering, the indications offered by the two algorithms are quite similar. This provides a cross-validation for both of them. The second conclusion is that RBFNN enhanced by the centers adaptivity performs much better than that with unmoved centers and is surely more suitable for intraoperative SEP monitoring. In particular, that is proved by the inverse relation between the trends of the latency and of the urine bladder temperature: this relation would be absent without the centers adaptivity. The third consideration is that the RBFNN offers an excellent dynamics, as proved by the analysis of Figs. 3 and 5. As a result, good tracking of both sudden and slow changes of the SEP waveform is provided. In particular, such capability shows a high statistical correlation between the amplitude trends of the detected SEPs and of the H-reflex, as expected because of the anatomical and physiological correlation of the two signals. Not only are the falls and recoveries in amplitude or the latency peaks promptly detected, but also changes in the whole waveform morphology. These changes would call for more refined analyses. Moreover, the computational time required for the sweep-by-sweep learning is moderate, which is obviously important for real-time processing.

In conclusion, the careful evaluation of the proposed algorithm and the analysis of its results show that this RBFNN is particularly suitable for the real-time single-sweep detection of SEPs during intraoperative neuromonitoring and the advantages it entails make it particularly preferable to other methods.

## References


[1] J.-M. Guérit, "Neuromonitoring in the operating room: Why, when, and how to monitor?," *Electroenceph. Clin. Neurophys.*, vol. 106, pp. 1–21, 1998.

[2] R. E. Minahan, "Intraoperative neuromonitoring," *Neurologist*, vol. 8, pp. 209–226, 2002.

[3] M. R. Nuwer, E. G. Dawson, L. G. Carlson, L. E. A. Kanim, and J. E. Sherman, "Somatosensory evoked potential spinal cord monitoring reduces neurologic deficits after scoliosis surgery: Results of a large multicenter survey," *Electroenceph. Clin. Neurophys.*, vol. 96, pp. 6–11, 1995.

[4] A. C. Merzagora, F. Bracchi, S. Cerutti, L. Rossi, A. M. Bianchi, and A. Gaggiani, "A radial basis function neural network for single sweep detection of somatosensory evoked potentials," in *Proc. 26th Annu. Int. Conf. IEEE EMBS*, San Francisco, CA, 2004, pp. 427–430.

[5] L. Rossi, A. M. Bianchi, A. Merzagora, A. Gaggiani, S. Cerutti, and F. Bracchi, "Single trial somatosensory evoked potential extraction with ARX filtering for a combined spinal cord intraoperative neuromonitoring technique," *Biomed. Eng. Online*, vol. 6, p. 2, 2007.

[6] K. S. M. Fung, F. H. Y. Chan, F. K. Lam, and P. W. F. Poon, "A tracing evoked potential estimator," *Med. Biol. Eng. Comput.*, vol. 37, pp. 218–227, 1999.

[7] J. R. Balzer, R. D. Rose, W. C. Welch, and R. J. Sclabassi, "Simultaneous somatosensory evoked potential and electromyographic recording during lumbo-sacral decompression and instrumentation," *Neurosurgery*, vol. 42, pp. 1318–1324, 1998.

[8] L. Pelosi, J. Lamb, M. Grevitt, S. M. H. Mehdian, J. K. Webb, and L. D. Blumhardt, "Combined monitoring of motor and somatosensory evoked potentials in orthopaedic spinal surgery," *Clin. Neurophysiol.*, vol. 113, pp. 1082–1091, 2002.

[9] J. M. Guérit and R. A. Dion, "State-of-the-art of neuromonitoring for prevention of immediate and delayed paraplegia in thoracic and thoracoabdominal aorta surgery," *Ann. Thorac. Surg.*, vol. 74, pp. 1867–1869, 2002.

[10] E. Kandel, J. H. Schwartz, and T. M. Jessel, *Principles of Neural Science*. New York: McGraw-Hill, 2000.

[11] I. M. Jou, "The effects of lumbar nerve root transection in rats on spinal somatosensory and motor-evoked potentials," *Spine*, vol. 29, pp. 147–155, 2004.

[12] E. J. Hartman, J. D. Keeler, and J. M. Kowalski, "Layered neural networks with Gaussian hidden units as universal approximations," *Neural Comp.*, vol. 2, pp. 210–215, 1990.

[13] J. Park and I. W. Sandberg, "Universal approximation using radial-basis-function networks," *Neural Comp.*, vol. 3, pp. 246–257, 1991.

[14] S. Cerutti, G. Baselli, D. Liberati, and G. Pavesi, "Single sweep analysis of visual evoked potentials through a model of parametric identification," *Biological Cybern.*, vol. 56, pp. 111–120, 1987.

[15] P. Laguna, O. Meste, P. W. Poon, P. Caminal, H. Rix, and N. T. Thakor, "Adaptive filter for event-related bioelectric signals using an impulse correlated reference input: Comparison with signal averaging technique," *IEEE Trans. Biomed. Eng.*, vol. 39, no. 10, pp. 1032–1044, Oct. 1992.

[16] D. O. Walter, "*A posteriori* "Wiener filtering" of average evoked response," *Electroenceph. Clin. Neurophysiol.*, vol. 27, pp. 61–70, 1969.

[17] H. J. Heinze and H. Kunkel, "ARMA-filtering of evoked potentials," *Meth. Inf. Med.*, vol. 33, pp. 29–36, 1984.

[18] M. V. Spreckelsen and B. Bromm, "Estimation of single-evoked cerebral potentials by means of parametric modeling and Kalman filtering," *IEEE Trans. Biomed. Eng.*, vol. 35, no. 9, pp. 691–700, Sep. 1988.

[19] B. Widrow, J. R. Glover, J. M. McCool, J. Kaunitz, C. S. Williams, R. H. Hearn, J. R. Zeidler, E. Dong, Jr., and R. C. Goodlin, "Adaptive noise canceling: Principles and applications," *Proc. IEEE*, vol. 63, no. 12, pp. 1692–1716, Dec. 1975.

[20] M. Schieppati, "The Hoffmann reflex: A means of assessing spinal reflex excitability and its descending control in man," *Prog. Neurobiol.*, vol. 28, pp. 345–376, 1987.

[21] W. Gersch, "Spectral analysis of EEG's by autoregressive decomposition of time series," *Math Biosci.*, vol. 7, pp. 205–222, 1970.

[22] S. Cerutti and D. Liberati, "Autoregressive modeling and filtering of EEG signal generating mechanism in patients under surgical interventions," *Model. Simulat. Contr.*, vol. 2, pp. 11–23, 1985.

[23] A. Papoulis, *Probability and Statitics*. Upper Saddle River, NJ: Prentice-Hall, 1990.

[24] J. E. Fitzgerald, C. J. Griffiths, K. W. Mitchell, M. A. Leonard, M. Gibson, and C. K. McKnight, "The effect of changes in epidural temperature on spinal evoked potentials during scoliosis surgery," in *Proc. 5th Int. Symp. Spinal Cord Monitoring*, London, U.K., 1992, pp. 117–124.



**Anna C. Merzagora** (S'04) received the M.S. degree in biomedical engineering from the Polytechnic University of Milan, Milan, Italy, in 2004, working in cooperation with the Neurophysiology Laboratory at Institute of Human Physiology, University of Milan Medical School. She is currently working toward the Ph.D. degree in biomedical engineering at Drexel University, Philadelphia, PA.

She is listed as a co-inventor in a patent pending about the new "Method and Equipment for Monitoring the Functionality of Spinal Cord." She is presently involved in the development of the application of functional near-infrared spectroscopy to cognitive sciences. Her interests include biosignal processing, neuroengineering, bioimaging.

**Francesco Bracchi** was born in Milan, Italy, on March 10 1938. He studied medicine and surgery in Milan and received the M.D. degree in 1963.

He has been Assistant at the Institute of Human Physiology, University of Milan Medical School, Milan, and then Senior Lecturer of Physiology from 1971 to 1985. Since 1985, he is Professor of Human Physiology at the same university. He worked with NASA on different occasions as Fellow of the National Academy of Sciences and carried out research at the Ames Research Center, Moffett Field, CA, on the vestibular system. As co-principal investigator he participated in the space vestibular experiment OFO-A at Wallops Island, VA, and at Ames Research Center. From 1977 to 1979, he was a Visiting Professor at the University of Pittsburgh, Pittsburgh, PA. He developed a method and equipment for monitoring the functionality of the spinal cord (Pat. Pend.) in cooperation with L. Rossi and A. Merzagora. His main fields of interest are the monitoring of nervous functions during surgery and medical electronics.

In 1983, Dr. Bracchi won an award from NASA for the development of a microprocessor-based neural pulse wave analyzer.

**Sergio Cerutti** (S'97–M'81–F'02) received the Laurea degree in electronic engineering from the Polytechnic University, Milan, Italy, in 1971.

From 1982 to 1990 he was Associate Professor of Biomedical Engineering with the Department of Biomedical Engineering at the Polytechnic University, where he is currently (since 1994) Professor of Biomedical Signal and Data Processing. From 1990 to 1994, was also Professor of Biomedical Engineering with the Department of Computer and System Sciences of the University of Rome "La Sapienza". His research activity is mainly dedicated to various aspects of biomedical signal processing and modelling related to the cardiovascular system and in the field of neurosciences. He is the author of various papers and books on these topics published in international scientific literature. He spent over a year as a Visiting Professor at the Massachusetts Institute of Technology (MIT) and Harvard School of Public Health, Boston, MA.

Dr. Cerutti was a member of AdCom of IEEE-EMBS (1992–1996) as Representative of Region 8. He is Chairman of the Biomedical Engineering Group of the Italian Association of Electrical Engineering (AEI) and is a member of IEEE-AEI, IFMBE-AIIMB, ESEM, IEC-CEI and other international and national scientific associations.

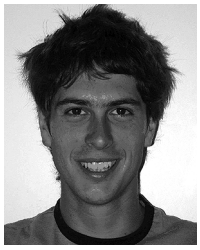

**Lorenzo Rossi** was born in Milan, Italy, in 1978. He received the B.E. degree in 2002 and is currently working toward the Ph.D. degree in the Department of Biomedical Engineering, Politecnico of Milan.

His research interests are biomedical electronics and information technology.

**Alberto Gaggiani** received the Diploma degree in chemistry, the Laurea degree in pharmacy and the M.D. degree in medicine and surgery.

Since 1988, he has been lecturing on subjects pertaining to chemistry, biochemistry, and endocrinology in the courses of Human Physiology at the University of Milan Medical School. Since 1999, he has been lecturing on anatomy, biochemistry, and endocrinology in the courses of Physiology of the Department of Biomedical Engineering of the Politecnico of Milan. He is consultant at the Institute of Human Physiology, the University of Milan Medical School, on neuromonitoring data analysis and on the action of the anesthesia drugs on spinal reflexes and EEG signal.

Dr. Gaggiani is a Specialist in Human Reproduction Pathology.

**Anna Maria Bianchi** (M'93) received the Laurea degree from the Polytechnic University, Milan, Italy, in 1987.

From 1987–2000, she was a Research Assistant with the Laboratory of Biomedical Engineering at the IRCCS, S. Raffaele Hospital, Milan, where her scientific and research activity was in connection with the Department of Biomedical Engineering, the Polytechnic University. Since 2001, she is a Research Assistant with the Department of the Biomedical Engineering, the Polytechnic University, where she is now Assistant Professor of Fundamentals of Electronic Bioengineering. Her research interests are mainly related to biomedical signal processing aimed to improve their information content, define new interpretative models of the biological systems and phenomena under examination. Applications are mainly in the cardiovascular field, with particular focus on control models of the principal variables and the autonomic regulation; the study of the neurosensorial system, mainly related to the single sweep analysis of the evoked potentials, to multichannel EEG recordings (EEG and EP mapping) and to the evaluation of the dynamical interactions in the EEG signal in particular situations such as learning, anesthesia, and motor tasks in normal subjects and in patients affected by epilepsy or dyslexia. Recently, her research is focused on the interactions between the central nervous system and the autonomic nervous system. She is the author of many scientific papers in international journals. She has participated in various research projects (national and international) in the field of biomedical engineering and is referee of many international journals.